Optik 127 (2016) 90–95

Contents lists available at ScienceDirect

Optik

journal homepage: www.elsevier.de/ijleo

Phase retrieval method from multiple-wavelength holograms for in-line holography

Yan Li*, Wen Xiao, Feng Pan

Key Laboratory of Precision Opto-mechatronics Technology, Ministry of Education, Beihang University, Beijing 100191, China

ARTICLE INFO

Article history:
Received 16 December 2014
Accepted 9 October 2015

Keywords:
Phase retrieval
Multiple-wavelengths
In-line digital holography

ABSTRACT

We propose two phase retrieval methods based on multiple diffraction intensity patterns recorded at different illumination wavelengths using in-line digital holography in which the appropriate constraints are imposed both on the hologram plane and object plane. A synthetic wavelength is used to retrieve wrap-free phase distributions with a much extended vertical measurement range; thus the reconstructed phase distribution directly provides the height distribution of the surface of the sample after eliminating the twin image. In comparison with previous research, the proposed method requires a fewer number of illumination wavelengths and has a faster rate of convergence, which is demonstrated by the simulation and experimental results.

1. Introduction

In-line digital holography, which had its origins in Gabor holography [1], is the most simplified holographic recording architecture: the scattered object beam and the unscattered reference beam propagate in the same direction and form the interference pattern downstream, thus no extra reference beam is required. Compared with off-axis digital holography, the more compact in-line scheme has a larger field of view, and becomes less sensitive to external perturbation and completely utilizes the space-bandwidth product of the detector. Therefore, it has been applied in many fields including the investigation of living cells [2] and particle field imaging [3]. However, both the defocused conjugate images and zero-order autocorrelation are superimposed on the real image of the object in the reconstruction process [4], which blurs the real image and degrades the measurement accuracy.

Various efforts have been made to solve the twin-image problem of on-axis digital holography (DH), for instance, by adopting phase retrieval algorithms, which can separate the real image from the unwanted conjugate image by involving iterative diffraction propagations back and forth between the object and the recording domains. For some algorithms, the amplitude of a single hologram is imposed on the recording plane as the constraint, and the convergence is guaranteed via other constraints, i.e. finite transmission [5–7] or finite support [8,9] on the object plane. Approaches have also been proposed without imposing any constraint on the object plane in which iterations are conducted along consecutive recording planes obtained from displacing the camera at different parts of the object [10–12] or distance [13–15]. However, the methods above are available only for the determination of the phase modulo 2π, and in some cases this is not sufficient. For objects that have a greater optical thickness variation than the wavelength, the phase images are wrapped in the range of $(-\pi, \pi]$ radians after arctangent calculation [16]. Although the unwrapping height can be extended by an infrared [17] and terahertz beam [18], the lack of corresponding optical components and decreased spatial resolution restrain further application of the longer illumination wavelengths. Bao et al. presented the phase retrieval technique based on multiple wavelengths, which extended the range of measurement, but its iterative algorithms use the square module constraint on the recording plane without imposing any constraint on the object plane, the convergence of which is very likely to be limited to local minimum. Thus, it requires a large number of illumination wavelengths and iterations to achieve high retrieval accuracy [19,20].

In this paper, two phase retrieval methods for multiple-wavelength in-line digital holography are proposed in which an iteration calculation is performed via in-line holograms recorded at four different wavelengths by a tunable laser. In this approach, a synthetic wavelength is used to calculate the wrap-free phase distributions, as in two-wavelength interferometry [16], and the appropriate constraints are imposed on both the hologram plane and object plane. Thus, the correct complex field distribution is retrieved at a faster rate of convergence and better elimination effect with a fewer number of wavelengths compared to those of

* Corresponding author. Tel.: +86 0182339736; fax: +86 0182339736.
E-mail address: liyanxing0514@163.com (Y. Li).

http://dx.doi.org/10.1016/j.ijleo.2015.10.017
0030-4026/

previous research [19,20]. Moreover, a more accurate unambiguous unwrapped phase distribution with a much extended measurement range is achieved by means of synthetic wavelength; thus, the reconstructed phase distribution can directly provide the height distribution of the surface of the sample. The feasibility of this method is validated by numerical simulations and related experiments.

2. Iterative algorithm

2.1. Phase retrieval method using single sequence holograms (PRSSH)

Four digital holograms were recorded at four illumination wavelengths (marked as λ_{11}, λ_{12}, λ_{21}, λ_{22}), and were divided into two groups. The wavelength interval between λ_{11} and λ_{21} should be the same as that of λ_{12} and λ_{22}. The main iterative procedures are as follows:

(1) An initial guessed phase $\phi_{\lambda_{11}}(x, y)$ is assumed at the beginning of the iterative calculation, where (x, y) is the coordinate in the hologram plane with recording distance z at the recording wavelength λ_{11}. $\phi_{\lambda_{11}}(x, y)$ multiplies the square roots of the normalized hologram, which is carried out by dividing the hologram $H_{\lambda_{11}}(x, y)$ by its corresponding background image $G_{\lambda_{11}}(x, y)$ in this plane, to yield the complex amplitude distributions $U_{\lambda_{11}}(x, y)$ at this plane:

$$U_{\lambda_{11}}(x, y) = \sqrt{\frac{H_{\lambda_{11}}(x, y)}{G_{\lambda_{11}}(x, y)}} \exp\left[j\phi_{\lambda_{11}}(x, y)\right]. \tag{1}$$

(2) $U_{\lambda_{11}}(x, y)$ propagates back to the object plane with the distance z by the angular spectrum propagation (ASP) integral [21], which is valid for short-distance propagations and keeps the same image size when the reconstruction distance changes:

$$\begin{aligned} U_{\lambda_{11}}(x_o, y_o) &= \mathrm{ASP}_{-z}\left[U_{\lambda_{11}}(x, y)\right] \\ &= A_{\lambda_{11}}(x_o, y_o) \exp\left[j\phi_{\lambda_{11}}(x_o, y_o)\right], \end{aligned} \tag{2}$$

where (x_o, y_o) is the coordinate in the object plane, $A_{\lambda_{11}}(x_o, y_o)$ and $\phi_{\lambda_{11}}(x_o, y_o)$ are the amplitude and phase distributions of $U_{\lambda_{11}}(x_o, y_o)$ in the object plane, respectively.

(3) The complex amplitude distributions in the object plane require two constraints. Due to the positive absorption of the object, the amplitude in the object plane should not exceed 1. The interference between the twin image and the unscattered wave results in these emerging negative absorptions; therefore, the amplitude of those regions with values larger than 1 should be replaced as follows [15]:

$$U'_{\lambda_{11}}(x_o, y_o) = \begin{cases} U_{\lambda_{11}}(x_o, y_o) & A_{\lambda_{11}}(x_o, y_o) \le 1 \\ 1 & \text{otherwise} \end{cases}. \tag{3}$$

(4) The phase of $U'_{\lambda_{11}}(x_o, y_o)$ is converted for the illumination wavelength λ_{12}, while the amplitude of $U'_{\lambda_{11}}(x_o, y_o)$ will be reserved:

$$\begin{aligned} \phi_{\lambda_{12}}(x_o, y_o) &= \frac{\lambda_{11}}{\lambda_{12}}\phi'_{\lambda_{11}}(x_o, y_o) = \frac{\lambda_{11}}{\lambda_{12}}\phi'_{\mathrm{unw}\_\lambda_{11}}(x_o, y_o) \\ &\quad + \frac{\lambda_{11}}{\lambda_{12}}N(x_o, y_o)\cdot 2\pi, \end{aligned} \tag{4}$$

where $\phi'_{\mathrm{unw}\_\lambda_{11}}(x_o, y_o)$ is the phase distribution that $\phi'_{\lambda_{11}}(x_o, y_o)$ subtracts integral wavelengths, and $N(x_o, y_o)$ is the unknown nonnegative integer numbers at a point (x_o, y_o). $\phi_{\lambda_{12}}(x_o, y_o)$ should be still wrapped in the range of $(\pi, -\pi]$ radians in the iterative propagations; therefore, the phase of those regions where values larger than π or lower than $-\pi$ should be subtracted 2π ($\ge \pi$) or added 2π ($\le -\pi$).

Then, the amplitude and phase yielding wavefront are combined at the object plane:

$$U_{\lambda_{12}}(x_o, y_o) = \left|U'_{\lambda_{11}}(x_o, y_o)\right| \exp\left[j\phi_{\lambda_{12}}(x_o, y_o)\right] \tag{5}$$

(5) $U_{\lambda_{12}}(x_o, y_o)$ propagates forward to the hologram plane at the recording wavelength λ_{12}. The amplitude is replaced with the square root of the normalized hologram at this plane, while the phase distribution is extracted and used as the input value for the next iteration, starting at step (2). When the iteration processing of λ_{12} is completed, λ_{11} is used. The complex amplitude is updated and corrected during the iterations. Further iterations eventually lead to the elimination of the twin image, and more accurate phase distributions can be obtained. Then, the iterative procedures with the other group of wavelengths λ_{21} and λ_{22} proceed by the same calculations, as above. Finally, an unambiguous unwrapped phase distribution with a much extended measurement range can be obtained by the subtraction of these two groups' final phases, based on the principle of two-wavelength interferometry [16]. The continuous object surface height profile $h(x_o, y_o)$ can be calculated from the determined synthetic wavelength.

$$h(x_o, y_o) = \frac{\lambda_\Lambda \cdot \phi''_{\lambda_\Lambda}(x_o, y_o)}{2\pi n_\Delta}. \tag{6}$$

where $n_\Delta = n - n_0$ is the refractive index difference between the sample and the surrounding medium. Thus, the wavelength interval in each group should be arranged to guarantee that the synthetic wavelength optical path length exceeds the maximum height variation of the object surface to avoid phase unwrapping. In the phase retrieval method using single sequence holograms (PRSSH) method, the term $N(x_o, y_o)\cdot 2\pi$ is neglected during the calculation, since the value of $N(x_o, y_o)$ is unknown, which may introduce errors of a magnitude that depends on the height variation of the object's surface.

2.2. Phase retrieval method using double sequences holograms (PRDSH)

In order to avoid the limitations described in Section 2.1, a method has been developed with the synthetic wavelength used during the iterative propagations. The main procedures of the phase retrieval method using double sequences holograms (PRDSH) method are as follows:

(1) Two iterative calculations start respectively with two initial guessed phases $\phi_{\lambda_{n1}}(x, y)$ ($n = 1, 2$), where (x, y) is the coordinate in the hologram plane with recording distance z at the recording wavelength λ_{n1}. $\phi_{\lambda_{n1}}(x, y)$ multiply the square roots of the corresponding normalized holograms, respectively, which is carried out by dividing the holograms $H_{\lambda_{n1}}(x, y)$ by their corresponding background images $G_{\lambda_{n1}}(x, y)$ in this plane to yield two complex amplitude distributions $U_{\lambda_{n1}}(x, y)$ at these planes:

$$U_{\lambda_{n1}}(x, y) = \sqrt{\frac{H_{\lambda_{n1}}(x, y)}{G_{\lambda_{n1}}(x, y)}} \exp\left[j\phi_{\lambda_{n1}}(x, y)\right]. \tag{7}$$

(2) $U_{\lambda_{n1}}(x, y)$ propagate back to the corresponding object planes by the angular spectrum propagation (ASP) integral; the new complex amplitudes $U'_{\lambda_{n1}}(x_o, y_o)$ are modulated using the same object constraints as in step (2) in Section 2.1.

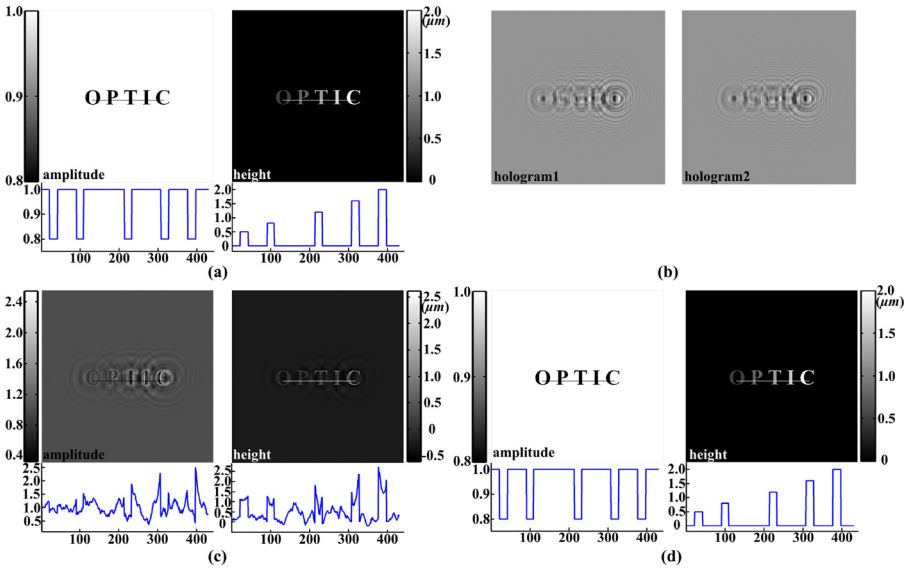

Fig. 1. Reconstruction images of a simulated 2D complex object: (a) original distribution in the object plane; (b) simulated hologram using conventional integral with wavelengths of 643.0 nm and 658.0 nm, respectively; (c) reconstruction by the method in Ref. [20]; and (d) the proposed approach after the 100th iteration.

(3) Calculate the synthetic phase from the two phases as follows:

$$\phi'_{\lambda_{\Lambda 1}}(x_o, y_o) = \begin{cases} \phi'_{\lambda_{11}}(x_o, y_o) - \phi'_{\lambda_{21}}(x_o, y_o) & \phi'_{\lambda_{11}}(x_o, y_o) > \phi'_{\lambda_{21}}(x_o, y_o) \\ \phi'_{\lambda_{11}}(x_o, y_o) - \phi'_{\lambda_{21}}(x_o, y_o) + 2\pi & \text{otherwise} \end{cases} \tag{8}$$

where $\phi'_{\lambda_{n1}}(x_o, y_o)$ are the phases of $U'_{\lambda_{n1}}(x_o, y_o)$, and $\lambda_{\Lambda 1}$ is the synthetic wavelength:

$$\lambda_{\Lambda 1} = \frac{\lambda_{11}\lambda_{21}}{(\lambda_{21} - \lambda_{11})}. \tag{9}$$

$\phi'_{\lambda_{n1}}(x_o, y_o)$ are converted for the illumination wavelength λ_{n2} by the unambiguous unwrapped phase distributions, respectively, according to Eq. (6), while the corresponding amplitudes will be reserved:

$$\phi_{\lambda_{n2}}(x_o, y_o) = \phi'_{\lambda_{\Lambda 1}}(x_o, y_o) \cdot \frac{\lambda_{\Lambda 1}}{\lambda_{n2}}. \tag{10}$$

(4) Combine the amplitudes and phases at each illumination wavelength yielding two wavefronts at each object plane.

$$U_{\lambda_{n2}}(x_o, y_o) = \left|U'_{\lambda_{n1}}(x_o, y_o)\right| \exp\left[j\phi_{\lambda_{n2}}(x_o, y_o)\right] \tag{11}$$

(5) $U_{\lambda_{n2}}(x_o, y_o)$ propagate forward to the hologram plane at the recording wavelength λ_{n2}, respectively. The amplitudes are replaced by the square root of the normalized holograms at these planes, while the phase distributions are extracted and used as the input values for the next iteration starting at step (2). As the synthetic wavelength is used to calculate the wrap-free phase during the iterative propagations, the unambiguous unwrapped phase distributions will be retrieved when the twin image is eliminated. However, in practice, the error would be continuously magnified while extending the range of unambiguous phase measurement [16]. For example, if the laser wavelengths of 643.0 nm and 658.0 nm are used to generate two phase maps, the resulting synthetic wavelength λ_Λ is 28.2 μm. If it is supposed that each phase measurement has an uncertainty of 0.1 rad, an optical thickness profile map obtained from a single wavelength will have an error of only about 10 nm, while the error of the extended range optical thickness profile will be approximately 449 nm. If the maximum height ($h_{\max}$) of the object is 20 μm, the error is 2.2 percent, while it will be increased to 22.5 percent for 2 μm, which is unacceptable. The comparisons of the convergence performances of PRSSH and PRDSH with the different maximum heights of the object are discussed in detail in Section 3.2.

3. Simulation

3.1. Simulation results and discussions

To validate the feasibility of the proposed algorithms, we simulated the in-line hologram using a synthetic two-dimensional complex object composed of five alphabets with different height distributions and a constant absorption of 20 percent of the incident coherent beam, as shown in Figs. 1(a) and 2(a). For PRSSH, the height distributions of the object were 0.5 μm, 0.8 μm, 1.2 μm, 1.6 μm and 2.0 μm, respectively, and for PRDSH they were 5 μm, 8 μm, 12 μm, 16 μm and 20 μm, respectively. A camera with 1024×1024 pixel of size $6.7 \times 6.7\ \mu m^2$ was utilized for recording. The holograms were numerically formed at distances of 140 mm from the object at four wavelengths of 643.0 nm, 644.0 nm, 658.0 nm and 659.0 nm, respectively. Thus, the corresponding synthetic wavelengths Λ in each group were 28.21 μm and 28.29 μm, which is larger than the maximum height of the object. The holograms simulated at wavelengths of 643.0 nm and 658.0 nm are displayed in Figs. 1(b) and 2(b). The method of phase retrieval using single sequence intensity patterns (PRSS) and double sequence intensity patterns (PRDS) in Ref. [20] were also used for comparison, and the reconstructed results after 100 iterations are shown in Figs. 1(c) and 2(c). The structures of the reconstructed images obtained from the method in Ref. [20] are fuzzy and distorted due to contamination of the twin image. The retrieved images from the proposed methods are shown in Figs. 1(d) and 2(d). The line scans show that the twin image has been completely removed after iterative calculation, and the reconstructed fields have reached their predefined value.

The convergence rate is the key indicator for iterative algorithms, which can be monitored in the iterations by the mean square error (MSE) defined as

$$\mathrm{MSE}^n = \frac{1}{M \times N} \sum_{\substack{\xi = 1, 2, \ldots, M \\ \eta = 1, 2, \ldots, N}} \left[\rho^n(\xi, \eta) - \rho_o(\xi, \eta)\right]^2 \tag{12}$$

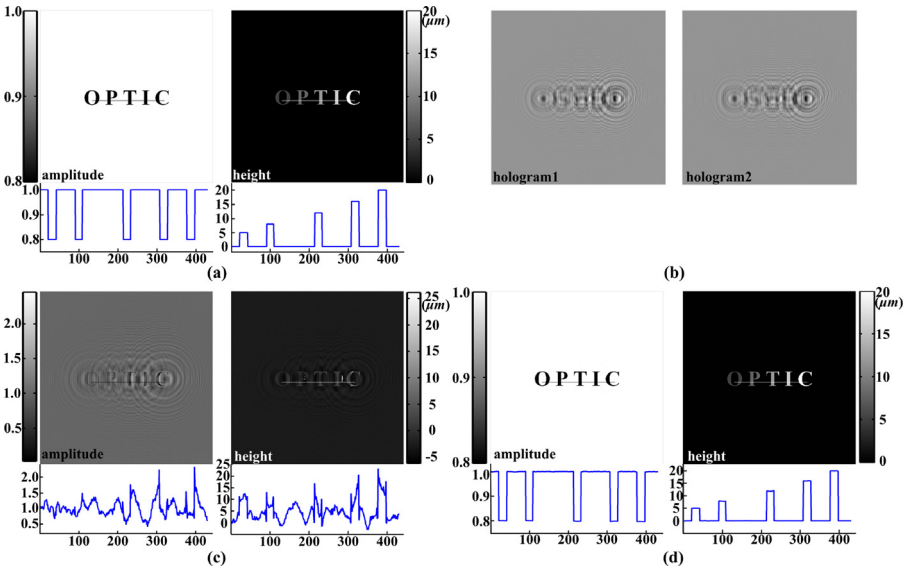

Fig. 2. Reconstruction images of a simulated 2D complex object: (a) original distribution in the object plane; (b) simulated hologram using conventional integral with wavelength of 643.0 nm and 658.0 nm, respectively; (c) reconstruction by the method in Ref. [20]; and (d) the proposed approach after the 100th iteration.

where $\rho^n(\xi, \eta)$ is the retrieved distributions, $\rho_o(\xi, \eta)$ is the original distribution of the object wavefront, and N, M denote the matrix sizes of the object domain. The corresponding comparison of the convergence rates are shown in Fig. 3. The logarithmic scale of MSE is used on the Y-axis label in order to express the conclusion more clearly. Comparing with the methods in Ref. [19], the proposed approaches have a faster rate of convergence and better elimination effect after the same number of iterations.

3.2. Comparisons of convergence performances between PRSSH and PRDSH

The pattern of "lena" was used for the simulation, the grey level of which indicates the height profile of a two-dimensional complex object, as shown in Fig. 4(a). Fig. 4(b)–(e) shows the result for the comparison of the convergence performances between the two methods when the maximum height of the object is different. According to these curves, the convergence behaviour of these two methods differs when the height variations of the object's surface become larger. When the maximum height (h_{max}) of the object is 2 μm, PRSSH has a faster rate of convergence and there is a better elimination effect after same number of iterations. When h_{max} is 12 μm, the convergence speed is almost the same, but the final result obtained by PRSSH is better. When h_{max} is increased to 15 μm, the convergence of PRDSH is faster than PRSSH, although these two methods reach the same final elimination effect. When h_{max} is 25 μm, PRSSH has a worse elimination effect, and the convergence speed is lower than PRDSH. On the other hand, when h_{max} is larger, the PRDSH method has a better result, while the PRSSH method works well for lower height. The comparisons show that the PRDSH method is more suitable for measuring objects with larger surface height variations. When the height variation of the object surface is not so large, the two methods should be chosen in order to balance the calculation speed and the final elimination effect.

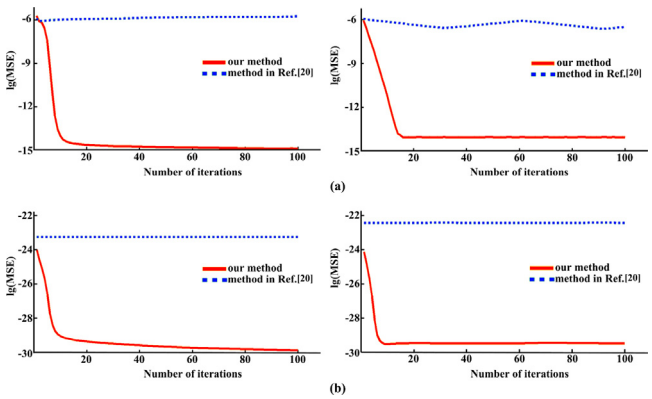

Fig. 3. Comparison of convergence rates of (a) amplitude and (b) height reconstruction of the 2D complex simulated object.

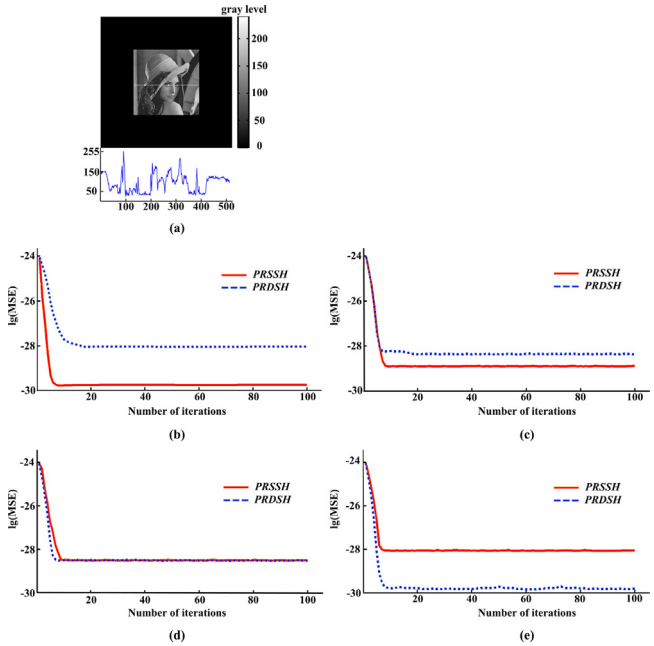

Fig. 4. (a) Test object used for the simulations of which the grey level indicates the height distributions (0–25 um); (b)–(e) comparison between the PRSSH and PRDSH methods: convergence curves when h_{max} = 2 μm (a); h_{max} = 12 μm (b); h_{max} = 15 μm (c); h_{max} = 25 μm (d).

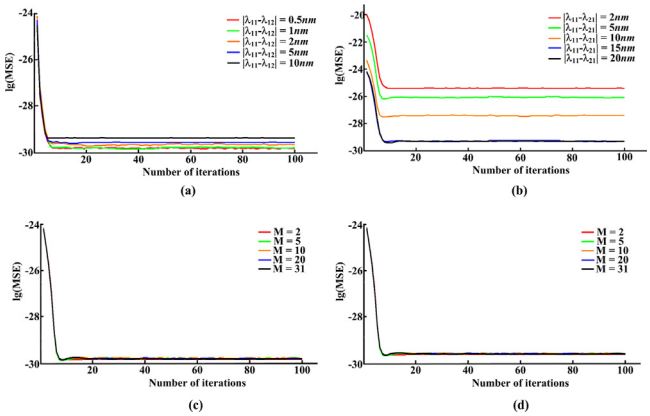

Fig. 5. Convergence performances of PRSSH and PRDSH under different conditions: (a) different wavelength intervals $|\lambda_{11} - \lambda_{12}| = 0.5$ nm, 1 nm, 2 nm, 5 nm and 10 nm in PRSSH; (b) different wavelength intervals $|\lambda_p - \lambda_q| = 2$ nm, 5 nm, 10 nm, 15 nm and 20 nm in PRDSH; (c) different numbers of holograms $M = 2$, 5, 10, 20, 31 in PRSSH; and (d) different numbers of holograms $M = 2$, 5, 10, 20, 31 in PRDSH.

3.3. Convergence performances under different conditions

The influence of experimental parameters on convergence performance was evaluated. The "lena" pattern was used with a maximum height of 2 μm for PRSSH and 20 μm for PRDSH. Fig. 5(a) presents the influence of wavelength interval on performance of PRSSH. The elimination effect is worse when the wavelength interval increases, while the rate of convergence is the same. The reason may be that the neglect of the term $N(x_o, y_o) \cdot 2\pi$ during the calculation introduces errors whose magnitude depends not only on the height variation of the object's surface, but also the wavelength interval. Thus, the wavelength interval should be kept small to get a better elimination effect in the PRSSH method. Fig. 5(b) shows the effect of the wavelength interval on the convergence performance of PRDSH. The curves represent the l g (MSE) versus the number of iterations when the wavelength interval $|\lambda_p - \lambda_q|$ is 2 nm, 5 nm, 10 nm, 15 nm and 20 nm. It is noticeable that the larger interval between the two wavelengths has a faster rate of convergence and better elimination effect after same number of iterations, while the curves with the wavelength intervals of 15 nm and 20 nm have the same convergence and elimination effect. Since a larger synthetic wavelength would amplify the noise, the two wavelengths should be far enough separated to satisfy the maximum level of phase noise [16]. Fig. 5(c) and (d) reveals that the performance of both PRSSH and PRDSH are not related to the number of used illumination wavelengths when constraints are imposed on both the hologram planes and object plane. When the number in each group of wavelengths was reduced from 31 to 2, the convergence speed was almost the same. On the other hand, the convergence of the algorithm in Ref. [20] requires no less than 10 illumination wavelengths.

4. Experimental analysis

Experiments were performed in order to verify the method. The tunable laser (Xperay-TL STD, Nanobase Inc, Korea) with a wavelength tuning range of between 640 nm and 675 nm was used as the light source. The beam derived from the laser source was collimated and expanded by a beam expander (composed of a spatial filter and collimating lens). A binary phase grating with 1 μm etching depth and a 300 μm period was used as the sample; the refractive index of the sample was approximately 1.5. A CMOS camera (Lumenera, LU-125M) with 1280 × 1024 pixel of size 6.7 × 6.7 μm^2 was utilized to record the hologram, but only 1024 × 1024 pixel were used to get an efficient FFT calculation. Four holograms were recorded consecutively at 100 mm downstream of the sample at A wavelength of 643.0 nm, 644.0 nm, 658.0 nm and 659.0 nm, respectively. The corresponding synthetic wavelength Λ in each group was 28.21 μm and 28.29 μm, and the exact distance was obtained via the

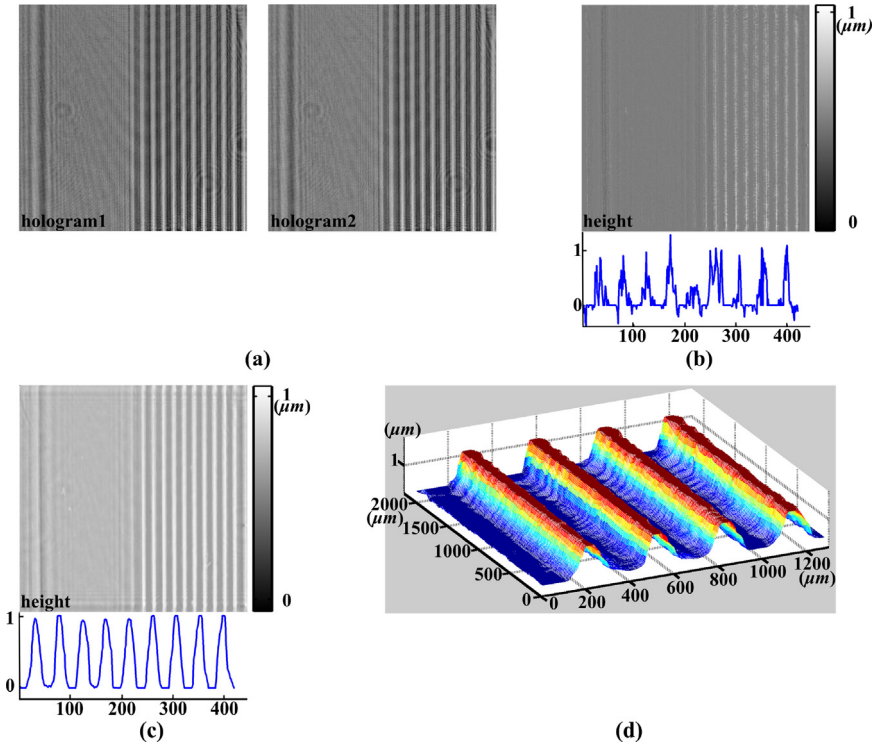

Fig. 6. Experimental result of binary phase grating: (a) normalized holograms recorded with wavelengths of 643.0 nm and 658.0 nm, respectively; (b) reconstruction by the method in Ref. [20]; and (c) retrieved distribution by the proposed approach after the 100th iteration; and (d) 3D perspective profile of the selected region indicated in (c).

Laplacian second-order differentiation auto-focusing method [22]. The corresponding backgrounds were taken in the same conditions in the absence of the object.

The holograms and the reconstruction results are shown in Fig. 6. As the etching depth of the binary phase grating is 1 μm, the PRSSH method is more suitable for measurement. Fig. 6(a) shows two in-line holograms recorded at the wavelengths of 643.0 nm and 658.0 nm with a distance of 100 mm. As Fig. 6(b) shows the object distribution is still obscured by the twin image after 100 iterations using the PRSS method in Ref. [20]. But after the same number of iterations, Fig. 6(c) clearly shows that the residual fringes are gone and the height distributions are truthfully recovered by proposed method. Fig. 6(d) depicts the 3D perspective profile for the cutout region indicated in Fig. 6(c). Both the line scan and 3D profile clearly show the peak and valley of the diffraction grating. The depth and period revealed by the reconstructed images match well with the grating's characteristics. The proposed method shows its applicability to quantitative height measurement.

5. Conclusion

This paper has presented two phase retrieval methods in which the iterative process was performed by four digital holograms recorded at wavelengths of 643.0 nm, 644.0 nm, 658.0 nm and 659.0 nm, respectively, to eliminate the twin image for in-line holography. By imposing constraints both on the recording planes and the object plane, the correct complex field distribution is retrieved iteratively. Based on the concept of the synthetic wavelength, the measurement range of the wrap-free phase has been extended to 28.21 μm and 28.29 μm. By comparing the iterative approaches without any constraint on the object plane in Ref. [20], the proposed methods show a faster rate of convergence and a better elimination effect. Moreover, the proposed methods can converge with fewer numbers of wavelengths than the approaches in Ref. [20] in which the convergence of the algorithms requires no less than 20 illumination wavelengths. The convergence performances of the two methods with the different maximum heights of the object have been theoretically analysed and discussed. The results shows that PRDSH has a faster convergence speed and achieves more accurate results when the object surface height is several times larger than the illumination wavelengths, while the PRSSH is more suitable for a lower height. Meanwhile, the performances of both methods have also been systematically demonstrated by simulation under different conditions. Since no reference beam or additional moving parts are needed in this technique, it is highly immune to noise or environmental disturbance and provides an alternative tool in profile measurement.

Acknowledgments

This work is supported by the National Natural Science Foundation of China (NNSFC) under Grant nos. 31000387 and 61177006, and the Innovation Foundation of BUAA for PhD Graduates (No. YWF-14-YJSY-038).

References

[1] D. Gabor, A new microscopic principle, Nature 161 (1948) 777–778.
[2] H. Ikeura-Sekiguchi, R. Kuroda, M. Yasumoto, et al., In-line phase contrast imaging of a biological specimen using a compact laser-Compton scattering-based X-ray source, Appl. Phys. Lett. 92 (2008) 131107.
[3] G. Pan, H. Meng, Digital holography of particle fields: reconstruction by use of complex amplitude, Appl. Opt. 42 (2003) 827–833.
[4] K. Nugent, Twin-image elimination in Gabor holography, Opt. Commun. 78 (1990) 293–299.
[5] G. Liu, P.D. Scott, Phase retrieval and twin-image elimination for in-line Fresnel holograms, J. Opt. Soc. Am. A: Opt. Image Sci. Vis. 4 (1987) 159–165.
[6] T. Latychevskaia, H.W. Fink, Solution to the twin image problem in holography, Phys. Rev. Lett. 98 (23) (2007) 233901-1–233901-4.
[7] T. Latychevskaia, H.W. Fink, Simultaneous reconstruction of phase and amplitude contrast from a single holographic record, Opt. Express 17 (2009) 10697–10705.
[8] G. Koren, D. Joyeux, Twin-image elimination in in-line holography of finite-support complex objects, Opt. Lett. 16 (1991) 1979–1981.
[9] L. Rong, Y. Li, S. Liu, W. Xiao, F. Pan, D. Wang, Iterative solution to twin image problem in in-line digital holography, Opt. Lasers Eng. 51 (2013) 553–559.
[10] J.M. Rodenburg, H.M.L. Faulkner, A phase retrieval algorithm for shifting illumination, Appl. Phys. Lett. 85 (2004) 4795–4797.
[11] P. Almoro, G. Pedrini, W. Osten, Aperture synthesis in phase retrieval using a volume-speckle field, Opt. Lett. 32 (2007) 733–735.
[12] F. Zhang, G. Pedrini, W. Osten, Phase retrieval of arbitrary complex-valued fields through aperture-plane modulation, Phys. Rev. A: At. Mol. Opt. Phys. 75 (2007) 043805–043808.
[13] G. Pedrini, W. Osten, Y. Zhang, Wave-front reconstruction from a sequence of interferograms recorded at different planes, Opt. Lett. 30 (2005) 833–835.
[14] Y. Zhang, G. Pedrini, W. Osten, H.J. Tiziani, Whole optical wave field reconstruction from double or multi in-line holograms by phase retrieval algorithm, Opt. Express 11 (2003) 3234–3241.
[15] L. Rong, F. Pan, W. Xiao, Y. Li, F.J. Wang, Twin image elimination from two in-line holograms via phase retrieval, Chin. Opt. Lett. 10 (2012) 060902-1–060902-3.
[16] J. Gass, A. Dakoff, M. Kim, Phase imaging without 2π ambiguity by multiple wavelength digital holography, Opt. Lett. 28 (2003) 1141–1143.
[17] R.J. Mahon, J.A. Murphy, W. Lanigan, Digital holography at millimetre wavelengths, Opt. Commun. 260 (2006) 469–473.
[18] L. Rong, T. Latychevskaia, D.Y. Wang, X. Zhou, et al., Terahertz in-line digital holography of dragonfly hindwing: amplitude and phase reconstruction at enhanced resolution by extrapolation, Opt. Express 22 (2014) 17236–17245.
[19] P. Bao, F. Zhang, G. Pedrini, W. Osten, Phase retrieval using multiple illumination wavelengths, Opt. Lett. 33 (2008) 309–311.
[20] P. Bao, G. Pedrini, W. Osten, Optical surface profile measurement using phase retrieval by tuning the illumination wavelength, Opt. Commun. 285 (2012) 5029–5036.
[21] K. Matsushima, H. Schimmel, F. Wyrowski, Fast calculation method for optical diffraction on titled planes by use of the angular spectrum of plane waves, J. Opt. Soc. Am. A: Opt. Image Sci. Vis. 20 (2003) 1755–1762.
[22] C. Guo, Q. Yue, G. Wei, L. Lu, et al., Laplacian differential reconstruction of in-line holograms recorded at two different distances, Opt. Lett. 33 (2008) 1945–1947.